Measurement of manufacture assembly stresses in thick composite components using a modified DHD method

Haixiao Hu[1,2], Shuxin Li[2,3,4*], Dongfeng Cao[3,4], Lisheng Liu[1,4] and Martyn Pavier[2*]

1. Hubei Key Laboratory of Theory and Application of Advanced Materials Mechanics, Wuhan University of Technology, Wuhan, China, 430070

2. Department of Mechanical Engineering, University of Bristol, Bristol, UK, BS8 1TR

3. State Key Laboratory of Advanced Technology for Materials Synthesis and Processing, Wuhan University of Technology, Wuhan, China, 430070

4. Institute of Advanced Materials and Manufacturing Technology, Wuhan University of Technology, Wuhan, China, 430070

Abstract

Understanding of the through-thickness distribution of assembly stresses caused by manufacture process-induced distortion (PID) in thick composite components is essential for safety and reliability assessment. Inspired by deep-hole drilling (DHD) method which is widely used to reconstruct residual stresses in thick metallic components, current research attempts to extend and modify the DHD technique to measure the manufacture assembly stresses in composite components. It is observed that the modified DHD technique can capture the global deformation profiles induced by the assembly stresses, but the previous DHD stress calculation method produces large stress errors. An integrating stress calculation method is then proposed by combining the homogeneous global and the layer-wise antistrophic stress-strain solutions. It is demonstrated that the assembly stresses calculated by the proposed integrating calculation method are significantly improved and it is feasible to measure the manufacture assembly stresses of thick composite components with the modified DHD technique.

Keywords: B. Internal stress; C. Finite element analysis (FEA); E. Assembly; Measurement technique

*Corresponding author:

E-mail address: lishuxin@whut.edu.cn (Shuxin Li), martyn.pavier@bristol.ac.uk (Martyn Pavier)

1. Introduction

Although carbon fiber reinforced plastic (CFRP) are widely used in new generation airframe structures such as for the Airbus A350XWB and Boeing 787, it is still difficult to manufacture precisely

large-scale CFRP structures and ensure their structural integrity during operation. Due to thermal-chemical-mechanical interactions, thermal expansion mismatch, chemical cure shrinkage and tool-parts interactions during the manufacturing process, composite components tend to deviate more from their designed geometrical configuration than metallic ones [1-4]. Counteracting these undesired manufacturing distortions and geometric deviations for composite structures is still a challenge for manufacturers. The typical solution is to use shimming to compensate for geometric deviation as shown in Fig. 1. The process of shimming involves test assembly of components, measuring the necessary shimming volume, disassembly, manufacture and application of shim, cure of shim and finally re-assembly of components. The cure of the shim alone takes about 10 hours at normal temperature (25℃). Consequently, assembly of composite components with shimming is time-consuming and expensive [5]. Furthermore, due to the complexity of the shimming process, incorrect shimming may occur resulting in undesired or unknown re-distribution of loads, potentially leading to premature failure during operation and costly repairs [6]. Assembly of composite structures using current shimming strategies has becomes a bottleneck to the production rate of aircraft [7,8].

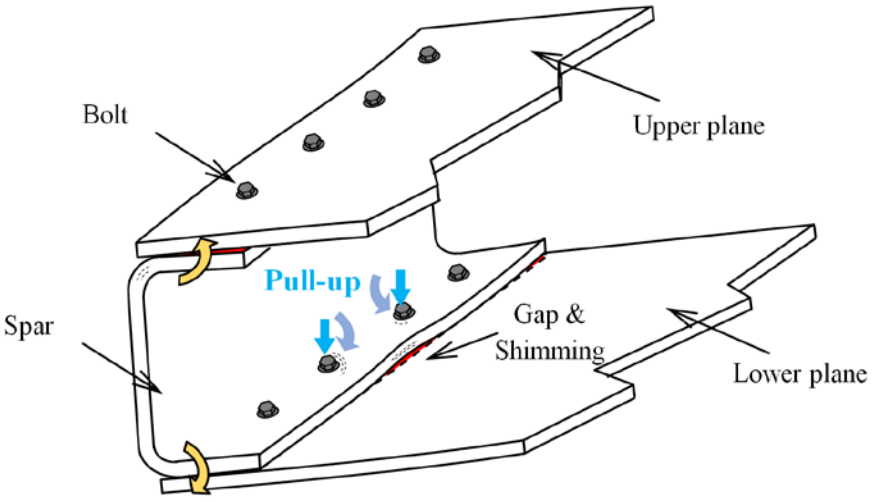

Fig. 1 Compensation of the fitting gaps in assembly of composite structures with shimming

In recent years, more attention has been given to achieving improved time and cost-effective

assembly of composite structures. One example is the European project - LOCOMACHS (LOw COst Manufacturing and Assembly of Composite and Hybrid Structures) [9]. The project focused on reducing or eliminating the most time-consuming operations such as temporary assembly to check gaps, shimming, dismantling and tool handling.

A related area of research is the influence of allowable gaps and shimming on the performance of composite structures. Yang [10] showed that different shimming materials would affect the flexural performance of composite plate joints while D'Angelo [11] found that the remaining gaps after assembly have an impact on the re-distribution of stresses. Söderberg [12] investigated how the variation in fixture and parts give rise to assembly stresses by FEM analysis. Wang [13,14] studied the static and fatigue failure of assembled composite laminates and concluded that assembly stresses is a critical issue in the structural integrity of composite structures. Most of this research has studied assembly issues for thin composite laminates. There is limited work on the assembly of the thick composite sections that are demanded for primary structures. The large number of layers in thick section composite laminates lead to large thickness fluctuations and geometric variation. In addition, the high stiffness lead to more complex and higher magnitudes of the through-thickness distribution of assembly stress. Understanding the through-thickness distribution of assembly stresses combined with reliable experimental measurement techniques is essential for structural assessment and optimized design of high-performance composite structures.

A number of experimental techniques have been developed to measure the strain and stress for engineering structures, such as traditional contact methods, extensometers and strain gauges for example, and contactless methods like Digital Image Correlation (DIC) [15,16]. However, these techniques only allow surface measurement rather than the through-thickness measurements that are important for thick section components.

Optical fibre sensors such as Fibre Bragg Grating sensors (FBGs) allow measurement of internal

strains in composite laminates [17,18]. Salvetti [19] embedded FBG sensors into laminates to study their response under low velocity impact and CAI behavior. Rito [20] monitored the internal strain of patch repairs with embedded FBG sensors. FBG sensors need to be pre-embedded in the specified positions before cure which makes it difficult to reconstruct the internal stresses of already-built structures. Hence, there is a need to explore sensing techniques to monitor the internal states of composite structures.

Deep-hole drilling (DHD) method is a well-established residual stress measurement method for thick section metallic materials and is particularly suitable to characterize the through-thickness profile of internal stresses. Initial works on DHD can be found in [21]. More recent improvements of the DHD method have been made by Smith and his co-workers [23-26] at the University of Bristol. Recently, attempts have been made to extend the DHD method to measure cure process induced residual stresses of composite laminates [27-29]. Due to the high level of interlaminar shear stress, it was found that the current DHD method cannot measure the cure process induced residual stress. However, the work indicated that the DHD method might be capable to measure the internal stresses induced by the external constrains or loading.

The current research attempts to extend and modify the DHD technique to measure the through-thickness profile of assembly stresses in order to address the challenges of understanding and qualification of assembly stresses in thick section composite components. Firstly, traditional DHD procedure for metallic materials and the recent advances of DHD techniques for composite materials with the extension of calculation method to orthotropic material are presented. Next, the feasibility of the modified DHD technique to measure the assembly stresses of composite components is explored. A four point bending condition was used to simulate the typical assembly object of closing gaps between components as shown in Fig. 1 [6,7]. It is observed that the previous DHD stress calculation method [29] produces substantial errors in the magnitude of the measured internal stresses.

Consequently, an integrating stress calculation methodology is proposed to improve the calculation accuracy, and both experimental and numerical simulation results demonstrate the feasibility of the modified DHD techniques to quantify the through-thickness distribution of assembly stresses in thick composite laminates.

2. Deep-hole drilling

2.1 Introduction to the method

Deep-hole drilling (DHD) is a semi-destructive method for residual stress measurement which is particularly suitable for thick components. Fig. 2 presents the main steps involved in the DHD procedure [23]. First, a reference hole is drilled through the thickness using a gun drill. Next, the diameter of the hole is measured using an air probe at different angular and through-thickness positions. Concentric trepanning is then carried out to release the residual stress from around the reference hole. Finally, the diameter of the hole is remeasured and the change in diameter used to calculate the residual stress. Front and back bushes are attached to the surfaces of the component to act as reference positions and support the core after trepanning. Typically, the DHD technique is carried out with a 3 mm diameter reference hole and a 10 mm trepan diameter [24]. For metallic components, the trepanning is carried out using EDM, but for composite materials a hole saw must be used.

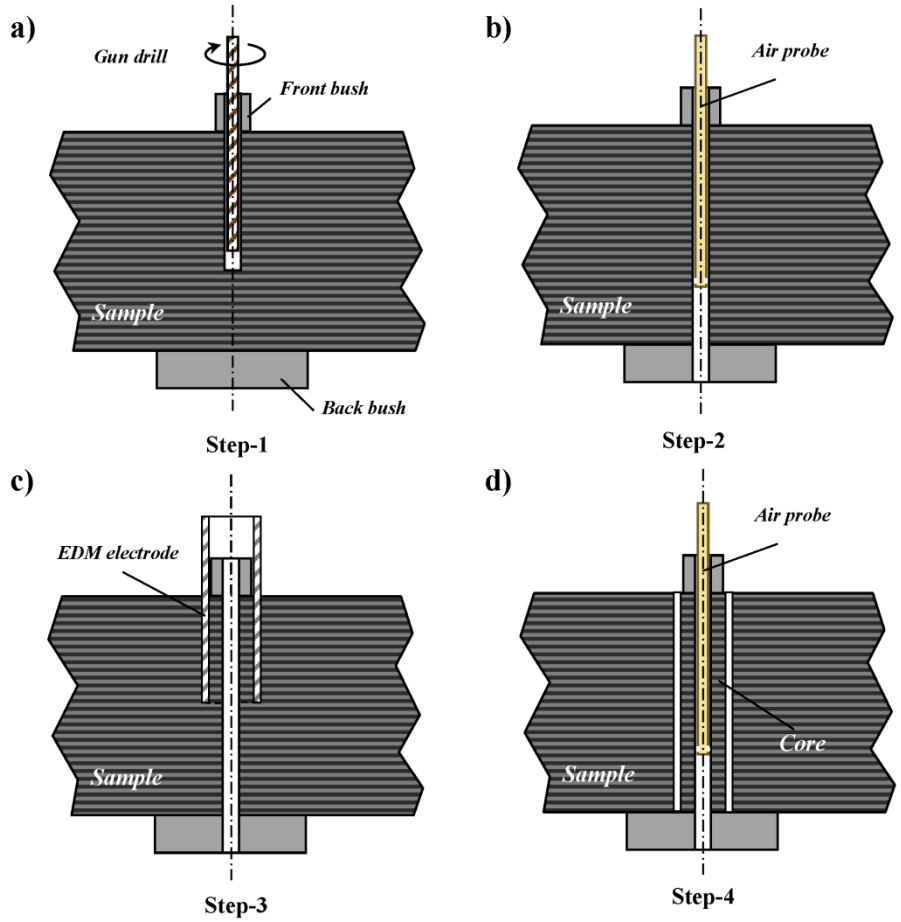

Fig. 2 Procedure of the DHD measurement: a) drilling of reference hole, b) measurement of reference hole, c) trepanning of core, d) remeasurement of reference hole [24]

2.2 Stress calculation for orthotropic materials

To obtain the residual stress in composite materials, it is assumed that a state of plane stress exists in the plane normal to the axis of the reference hole, the section is made up of independent blocks of plies with the same orientation and the residual stress in the core is completely released after trepanning [23-25].

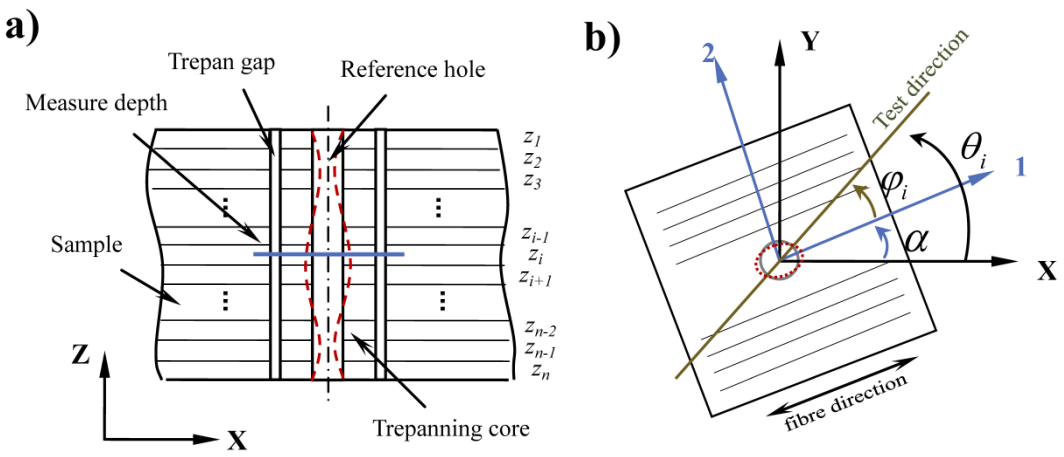

Fig. 3 Measurement of hole distortion by DHD method: a) cross-section view, b) top view

As shown in Fig. 3 a), the diameter of reference hole is measured at a set of n depths $Z=\{z_1,z_2,...z_n\}$ and a set of m angles $\theta=\{\theta_1,\theta_2,...\theta_m\}$, where $m\geq 3$. The depths are measured from the top surface of the laminate and the angles from a reference direction X, as shown in Fig. 3 b). At each depth, the hole distortion $\bar{u}|_{\theta=\theta_i}$ is calculated by,

$$\begin{bmatrix} \bar{u}|_{\theta=\theta_1} \\ \vdots \\ \bar{u}|_{\theta=\theta_i} \\ \vdots \\ \bar{u}|_{\theta=\theta_m} \end{bmatrix} = \begin{bmatrix} \left(d_{1,1}-d_{0,1}\right)/d_{0,1}|_{\theta=\theta_1} \\ \vdots \\ \left(d_{1,i}-d_{0,i}\right)/d_{0,\mathrm{i}}|_{\theta=\theta_i} \\ \vdots \\ \left(d_{1,\mathrm{m}}-d_{0,\mathrm{m}}\right)/d_{0,m}|_{\theta=\theta_m} \end{bmatrix} \tag{1}$$

where $d_{0,i}$ is the diameter of the reference hole at angle θ_i before trepanning and $d_{1,i}$ the diameter after trepanning.

For the ply at depth z_i with an orientation angle of α_i, Garza et al. [28,31] proposed that the stress components σ_{11}, σ_{22} and σ_{12} in the principal material directions can be calculated as,

$$\begin{bmatrix}\sigma_{11}\\ \sigma_{22}\\ \sigma_{12}\end{bmatrix}=-E_{11}M^{*}\bullet\begin{bmatrix}\bar{u}\,|_{\theta=\theta_1}\\ \vdots\\ \bar{u}\,|_{\theta=\theta_i}\\ \vdots\\ \bar{u}\,|_{\theta=\theta_m}\end{bmatrix} \tag{2}$$

where E_{11} is the elastic modulus in the fibre direction and M^{*} the pseudo-inverse of the distortion coefficient matrix M, derived from Lekhnitskii's analysis [31]

$$M=\begin{bmatrix} f_{\varphi_1} & g_{\varphi_1} & h_{\varphi_1}\\ \vdots & \vdots & \vdots\\ f_{\varphi_i} & g_{\varphi_i} & h_{\varphi_i}\\ \vdots & \vdots & \vdots\\ f_{\varphi_m} & g_{\varphi_m} & h_{\varphi_m}\end{bmatrix} \tag{3}$$

where φ_i denotes the angle between the fibre direction and the reference X direction, $\varphi_i=\theta_i-\alpha_i$, as shown in Fig. 3 b). The functions f_{φ_i}, g_{φ_i} and h_{φ_i} are given by

$$\begin{cases} f_{\varphi_i}=\dfrac{1}{2}\left[1+n_1-k\right]+\dfrac{\cos 2\varphi_i}{2}\left[1+n_1+k\right]\\ g_{\varphi_i}=\dfrac{1}{2}\left[\left(1+n_2\right)k^2-k\right]-\dfrac{\cos 2\varphi_i}{2}\left[\left(1+n_2\right)k^2+k\right]\\ h_{\varphi_i}=\left[\dfrac{E_{11}}{2G_{12}}+\dfrac{n_1\left(1+k\right)}{2}+k-\nu_{12}\right]\sin 2\varphi_i\end{cases} \tag{4}$$

where $\begin{cases} n_1=\sqrt{\left[2\left(\sqrt{E_{11}/E_{22}}-\nu_{12}\right)+E_{11}/G_{12}\right]}\\ n_2=\sqrt{\left[2\left(\sqrt{E_{22}/E_{11}}-\nu_{21}\right)+E_{22}/G_{12}\right]}\\ k=\sqrt{E_{11}/E_{22}}\end{cases}$

E_{11}, E_{22}, G_{12}, ν_{12} are the elastic constants of the unidirectional laminate.

3. Assessment of the accuracy of deep-hole drilling for measurement of assembly stress

Following the approach described by Garza et al. [29], experimental measurements have been

carried out to assess the ability of the DHD technique to measure accurately assembly stresses. Four-point bending loads were applied to composite laminates to simulate the generation of assembly stress. To simplify the test, a modified DHD technique was used where the measurement of the reference hole after trepanning in the standard DHD test is replaced by the measurement of the reference hole before loading. This procedure removes the influence of any cure stress existing in the laminate on the hole distortion. In addition to the physical measurement, a finite element simulation of a virtual DHD measurement was carried out to ~~carried out to~~ provide the reference data of assembly stresses.

3.1 Sample information

Samples were made from prepreg (M21/IMA-12K, Hexcel) and laminated by hand on an invar plate mould covered by release film. To eliminate manufacturing imperfection such as voids and wrinkles, the laminates were debulked for every four layers with the aid of vacuum during laminating. The prepreg stacks were covered by release cloth and a rubber cover plate which has small through thickness holes. Afterwards it was bagged and cured in an autoclave according to the curing processes recommended by the supplier. Two types of layup were used: layup L, $[[0_2/90_2]_{4S}]_S$, and layup M, $[[0_2/45_2/90_2/\text{-}45_2]_{2S}]_S$. The cured laminates were cut into specimens with a dimension of 240 mm×50 mm×11.52 mm using a diamond circular saw. The average ply thickness calculated based on the total thickness of the cured laminates is slightly lower than the normal ply thickness of 0.184mm as given in [35]. Consequently, the material properties especially the fiber dominated properties could be increase slightly. However, the calculated longitudinal modulus is increased to only about 2.2%, which is within the engineering tolerance for the DHD method. Two specimens were produced, one for each of the layups. A front bush and back bush made of bulk adhesive (Araldite 2015, Huntsman LLC) with a dimension about 10 mm×10 mm×6 mm and were bonded to the specimens as shown in Fig. 4. The bushes are used to prevent potential damages such peelings during the drilling operation since damages around the hole caused by the manufacturing of the reference hole can affect the accuracy of

measurements and stress prediction. The drilling parameters were also carefully selected to provide good finished quality of the reference holes. The front and back bush attached on the surfaces of the sample also provide continues measurements of the hole diameter to avoid the free edge effect of the surfaces with the DHD technique. The critical dimensions in the thickness direction are listed in Tab. 1.

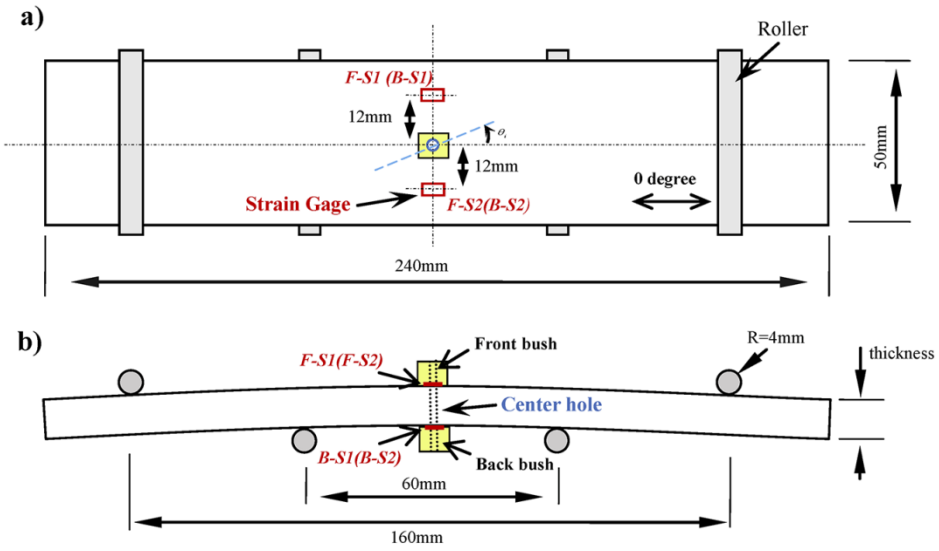

Fig. 4 Dimension of the four point bending sample: a) Top view, b) Side view.

Table. 1 Dimensions of tested samples

Type	L	M
Layup	$[[0_2/90_2]_{4S}]_S$	$[[0_2/45_2/90_2/-45_2]_{2S}]_S$
Thickness	11.45 mm	11.52 mm
Length of front bush	6.42 mm	4.79 mm
Length of back bush	6.54 mm	6.72 mm

A self-loading four-point bending fixture was used to apply loads to the specimen with a loading span of 60 mm and a support span of 160 mm. Four strain gauges (EP-08-031CF-120, Micro measurements) labeled F-S1, F-S2, B-S1 and B-S2, were bonded to the specimens aligned in the length direction as shown in Fig. 4.

3.2 Procedure of the physical DHD test

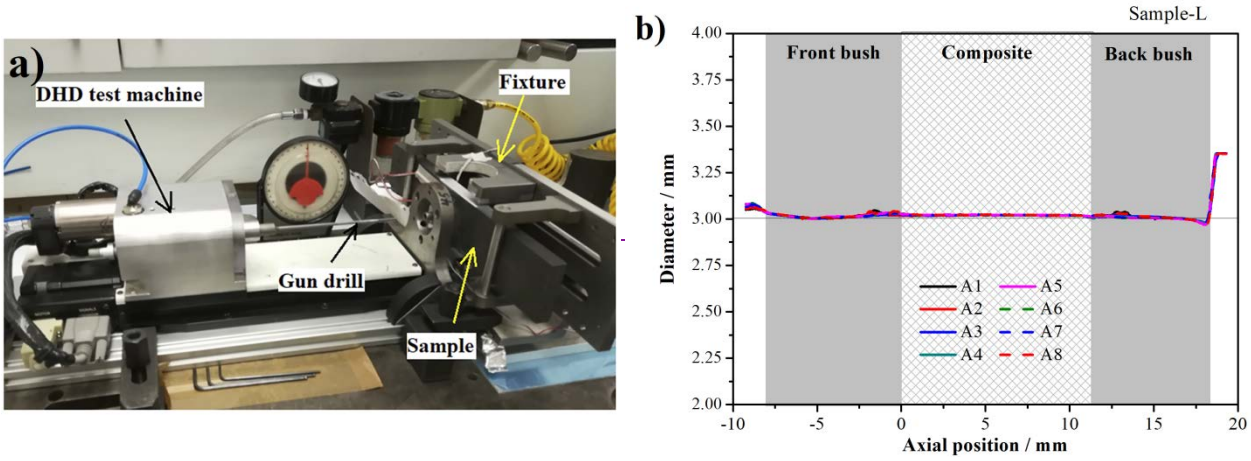

Fig. 5 Setup of the DHD test a) and the initial diameters measured before loading b)

To carry out the DHD measurement, special purpose equipment designed and manufactured by VEQTER Ltd, UK [32] was used. Fig. 5 shows the equipment in use and the initial diameters measured before loading . The test was conducted using the following procedure:

1) The specimen was located in the loading fixture and aligned with the DHD equipment.

2) A central hole was drilled through the whole thickness using a 3 mm diameter gun drill running at 1000 rpm and with a feed rate of 2mm/min.

3) After drilling, the specimen was allowed to cool to room temperature for 2 hours to release the heat generated during drilling.

4) Before measurement of the hole diameter, calibration of the air probe was carried out with precise ring gauges of different diameters.

5) The diameter of the central hole was measured by air probe for every 0.05 mm along the axis of the hole. The diameter was also measured at 8 angles with an increment of 22.5 degree at each axial location. The initial position of the rotation is defined in Fig. 4.

6) The load on the specimen was then increased by rotating the loading screw with an increment of displacement of 0.4 mm.

7) The air probe was re-calibrated as described in step 4.

8) The diameter of the central hole was re-measured as described in step 5.

Steps 6 to 8 were carried out 4 times. Therefore, measurements of the diameter of the hole were made before a bending load was applied to the specimen and after 4 levels of increasing bending load were applied, corresponding to displacements of the loading screw of 0.4, 0.8, 1.2 and 1.6 mm. These 4 levels of increasing bending load are referred to as load levels. Two samples for each layup were measured in DHD test and each sample was loaded and unloaded twice to check the repeatability and reliability. The test results show a good repeatability and consequently only one of the measurements for each layup was presented in section 3.4.

To quantify the loading precisely, strains were recorded at each increment using a strain indicator (Model P3, Micro measurements). From the measured change of diameter, the central hole distortion $\bar{u}|_{\theta=\theta_i}$ was calculated with Eq. (1) for each measurement angle through the thickness. Finally, the residual stress was calculated based on the calculation method described in Section 2. Since there are three unknown stresses and 8 measured distortions at each thickness, the matrix M is non-square and the problem is over specified. Consequently, a standard least square algorithm was developed and used here to obtain the optimum stress vector using Matlab. The elastic constants of unidirectional laminates for the composite material used in this study are obtained from [33] and are listed in Tab. 2.

Table. 2 Elastic constant of unidirectional laminates [33]

Property	E_{11}/GPa	E_{22}/GPa	E_{33}/GPa	G_{12}/GPa	G_{13}/GPa	G_{23}/GPa	ν_{12}	ν_{13}	ν_{23}
Value	143	7.89	7.89	3.92	3.92	2.76	0.33	0.33	0.43

3.3 Finite element simulation of a DHD measurement

In this section, a finite element simulation of the modified DHD test is described, using a three-dimensional model to predict the hole distortion and stress field. The finite element results will be compared with those from the experiment to assess the ability of the modified DHD approach for assembly stress measurement. Since the influence of the adhesive bushes on the measurement is small,

only the composite laminate is modelled. The finite element simulation was conducted using ABAQUS 6.17 with reduced integration solid brick elements type C3D8R. One element was used per layer in the thickness direction with a thickness of 0.36mm. The dimensions of the model are consistent with the physical test, as shown in Fig. 6. In the central hole region, a refined mesh was used with 64 elements in circumferential direction. The loading span s was 60 mm and the supporting span s' 160 mm to match the experimental dimensions. Loads were applied to the model by displacing nodes located at the support in the z direction. The precise level of displacement was determined by fitting the average value of the measured strain within the strain gauge area to be equal to that in the experiment.

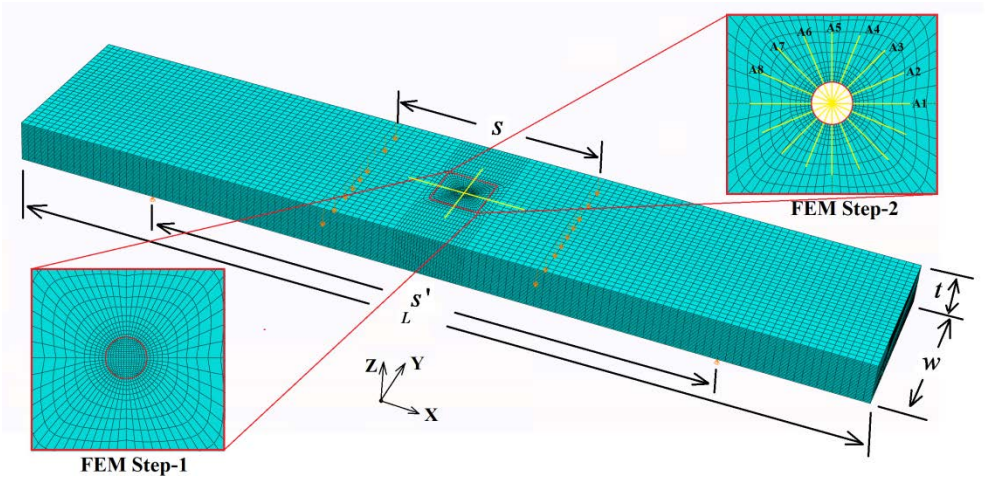

Fig. 6 FEA model used in the virtual investigation

In line with the proposed assembly stress measurement method, the finite element simulation was carried out in two steps. In the first step, a 3D model of the specimen without a central hole was used to calculate the stress field due to bending. The predicted stresses along the axis through the center of the specimen were taken to be the target value for the measurement of assembly stress. In the second step, the model was changed to one including the central hole. The changes in diameter of the hole for different orientations and through thickness positions to match those used in the experiment were predicted at different levels of loading. Finally, the predicted assembly stresses were calculated from the hole distortions following the approach described in section 2.2.

3.4 Experimental and simulation results

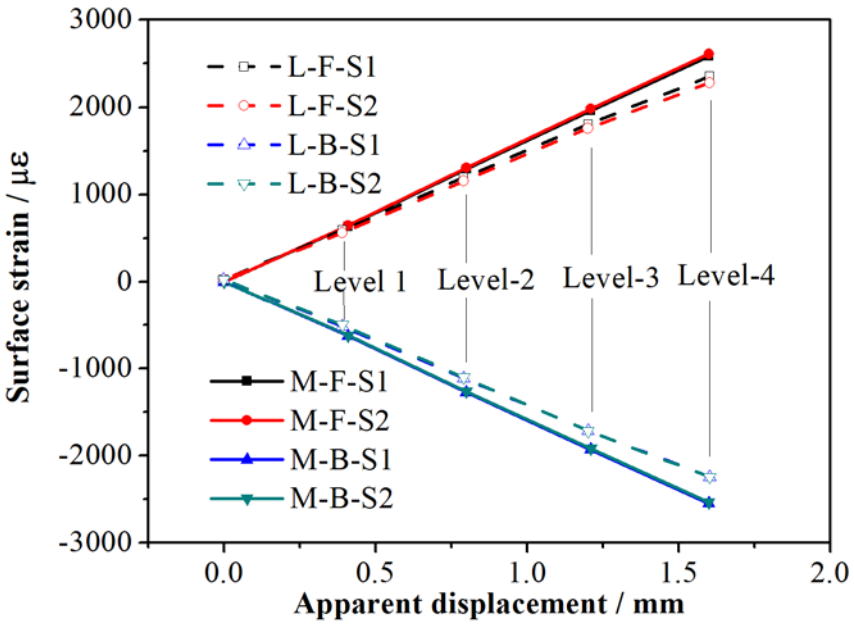

Fig. 7 Measured surface strains versus applied displacement with increasing load level.

The strain data measured from the strain gauges during the physical test are plotted versus screw loading displacement in Fig. 7 to confirm the loading conditions. It is observed that the strains increase linearly with displacement which supports that the use of linear elastic behavior in the experimental analysis and finite element simulations. Any possible nonlinear material response occurred near the hole will not affect the strain gages and will also not affect the global mechanical response which is the focus of this study. Furthermore, each sample was loaded and unloaded twice, and the good repeatability indicated that there was none, or negligible nonlinear material response occurred near the hole. The strain magnitudes of sample L are smaller than the ones of sample M. It is due to that the screw loading displacement is total displacement of sample and rig. Sample L which has a higher bending stiffness than sample M gives a smaller deformation. The strain measured on the tensile surface was slightly higher than that one on compressive surface with a difference of no more than 4%. Note that the screw loading displacement presented here is influenced by the deformation of the rig and by that of the specimen. Therefore the displacement cannot be used directly to define the load on

the finite element model, rather the strain gauge readings are used of this purpose.

The diameter changes at angle A1 measured from the physical test corresponding to the 4 steps of loading for sample L is plotted in Fig. 8 as example to illustrate the general features of the experimental results.

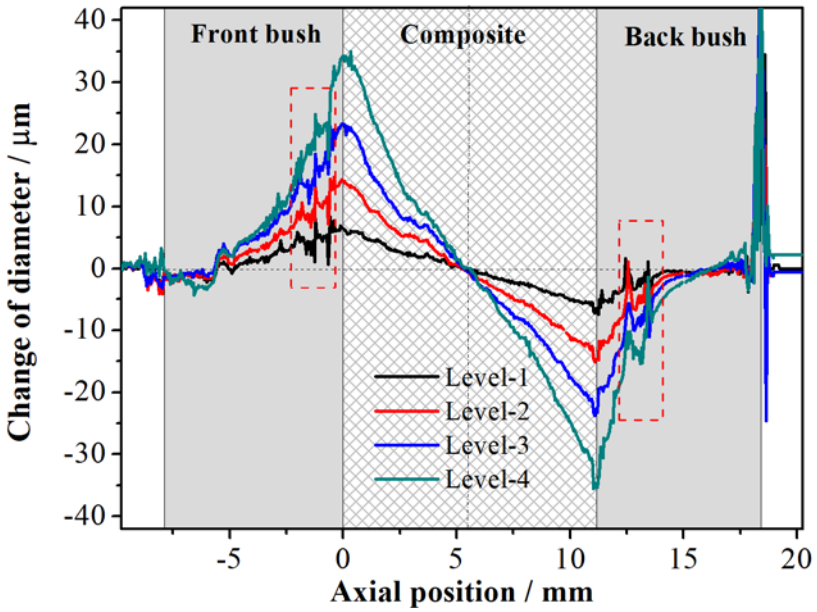

Fig. 8 Change of diameter at angle A1 (Sample L) with increasing load level

It is shown from Fig. 8 that the hole deformed continuously through the thickness. Nearly linear profile is observed at each level of loading in composite laminates region. The hole expanded at the front side and contracted at the back side as expected. At the mid-position of thickness, no obvious changes were observed which indicated that the neutral plane located near the mid-position. For the measurements in bushes, the change of diameter goes to zero at the free surface. The fluctuations within the bushes may be caused by voids.

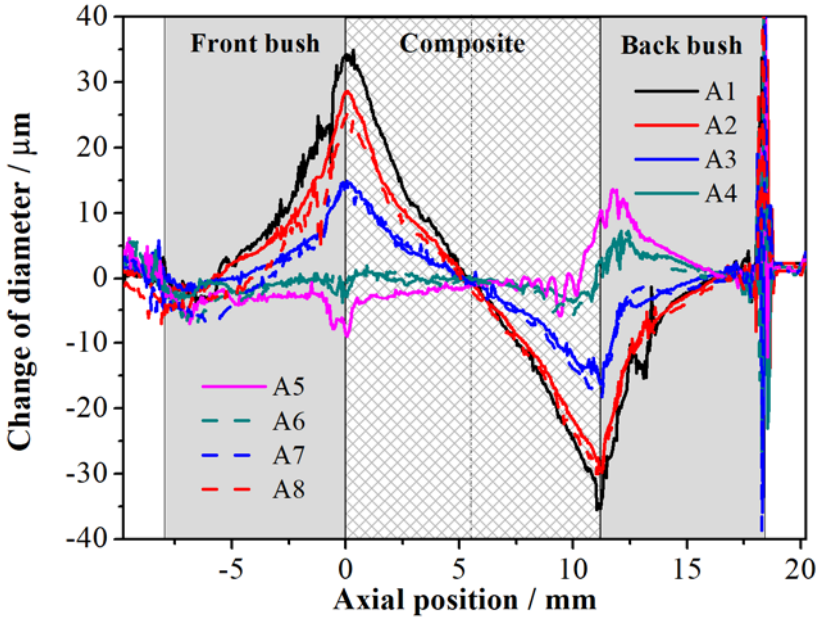

Fig. 9 Change of diameters at 8 angles for load level 4 (Sample L)

Fig. 9 presents the overall change of diameters around the central hole along thickness at 8 angles as defined in Fig. 6 for sample L at step 4 loading. As expected, central hole deformed symmetrically along the length direction with similar deformation profiles at the locations of A2 and A8, A3 and A7, as well as A4 and A6 respectively. At the angles of A1, A2, A3, A7 and A8, the hole expanded at front side and contracted at back side and an opposite tendency was observed at angles of A4, A5 and A6. Similar deformation profiles were also presented by sample M.

The changes of the hole diameter at the front and back surfaces of the composite laminates for load level 4 are plotted in Fig. 10 for both sample L and M.

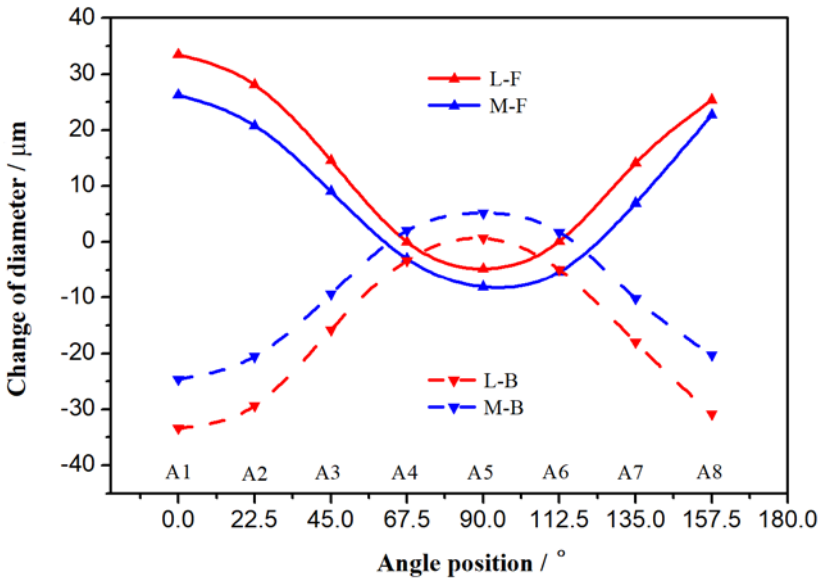

Fig. 10 Profiles of diameter changes at 8 angular positions for load level 4

The figure shows that similar profiles for the central hole deformation versus angular position were observed for both sample L and M. Sample L generally shows bigger deformation than sample M, indicating that the layup sequence has a significant influence on the magnitude of hole deformation. For an equal displacement load, the layup which has a higher global bending stiffness gives a larger amount of central hole deformation.

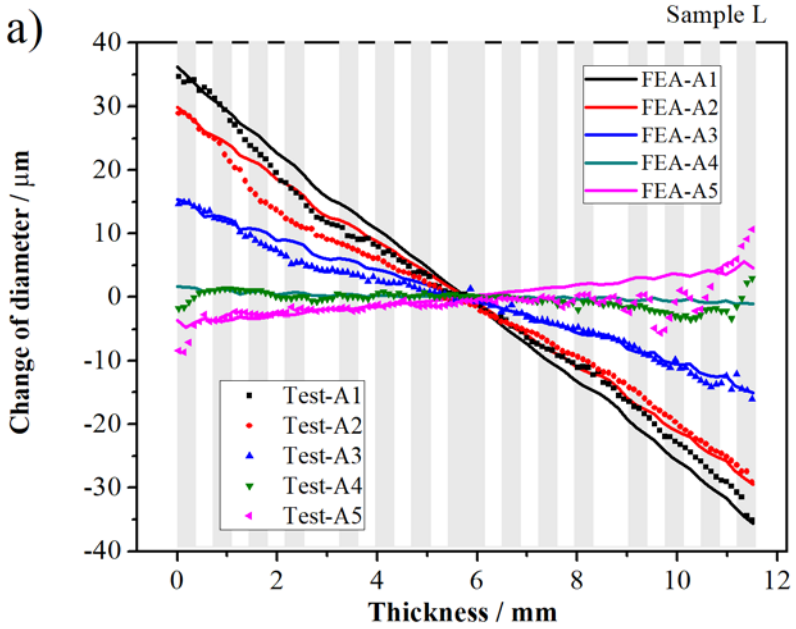

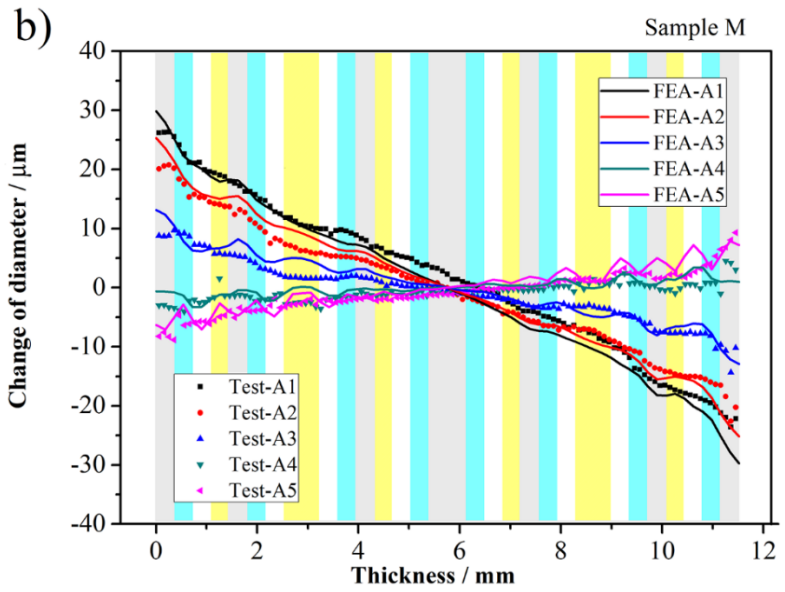

Fig. 11 Change of the diameters for load level 4 a) Layup L, b) Layup M (notes: 0° layer, 90° layer, 45° layer, -45° layer)

Fig. 11 provides comparisons of the changes of diameter obtained from physical DHD measurements and the virtual DHD numerical simulations for both layup L and layup M. Results are plotted for angular locations from A1 to A5. Results for angular location from A6 to A8 are not shown because they would lie over the A1 to A5 results, as indicated in Fig. 10. There is a generally good agreement between the experimental and the simulation results. For sample L, local variations were observed near the locations of 1/4 of thickness. This may be due to that the air probe is not aligned well with the central hole. In addition, the initial imperfection of the composite coupon such as the uniformity of the thickness of the layers and the finish surface of hole also affects the measurement [33]. However, since the global profile of the central hole distortion is focused in the current study to calculate the stress field, the influence of the local variation from the experimental measurement should be insignificant for the global verification of the modified DHD technique proposed.

Based on the results for the change of diameter obtained from experimental measurement and numerical simulation, the internal stress profiles of the composite laminates can be determined using

the calculation method described in section 2.2. The results of this calculation are compared in Fig. 12 for sample L and in Fig. 13 for sample M. The results labeled 'FEA calculation' are for the calculation of internal stresses based on the hole distortions at different angles obtained by the DHD FE simulation and the stress calculation method given in section 2.2. The results labeled 'Test calculation' are derived from the experimental measurements of the hole distortions at different angles with the same stress calculation method. There is generally good agreement between the stress profiles obtained from the FEA calculation and test measurements.

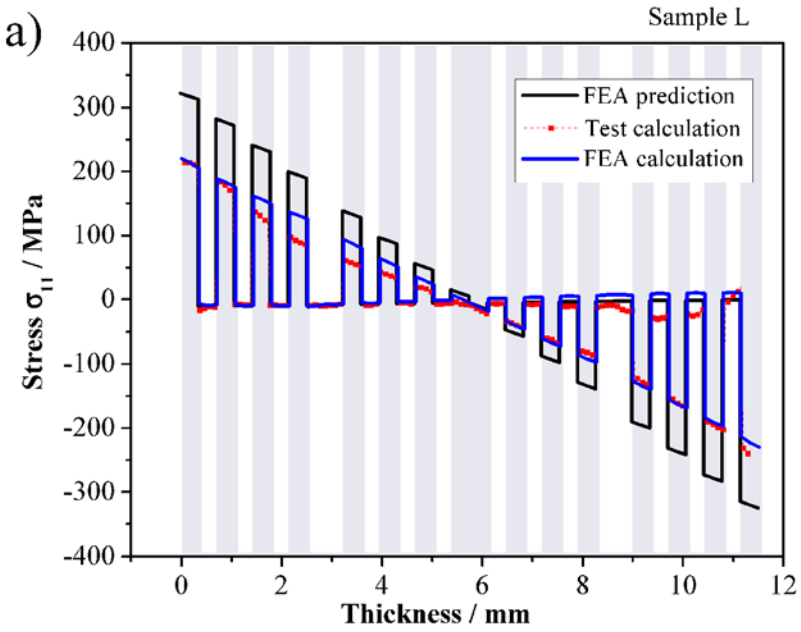

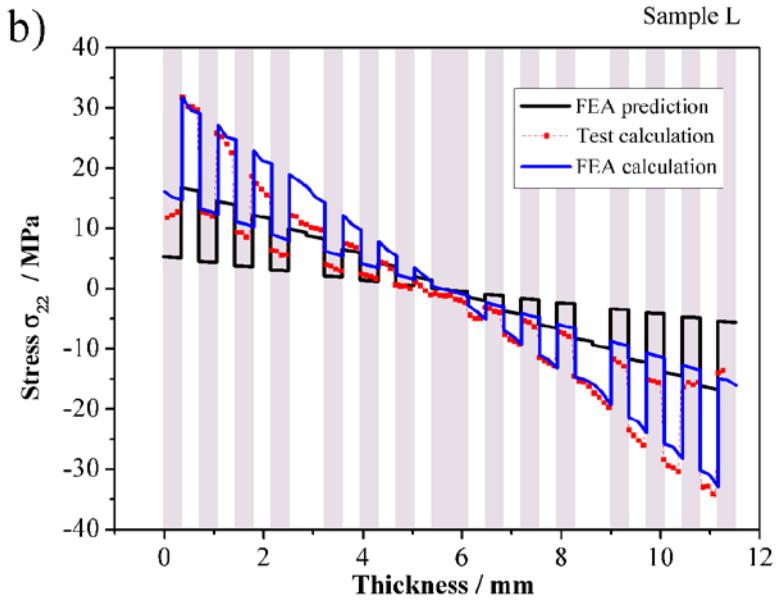

Fig. 12 Distribution of internal stresses at load level 4 for sample L: a) stress σ_{11}, b) stress σ_{22}

(notes: 0° layer, 90° layer)

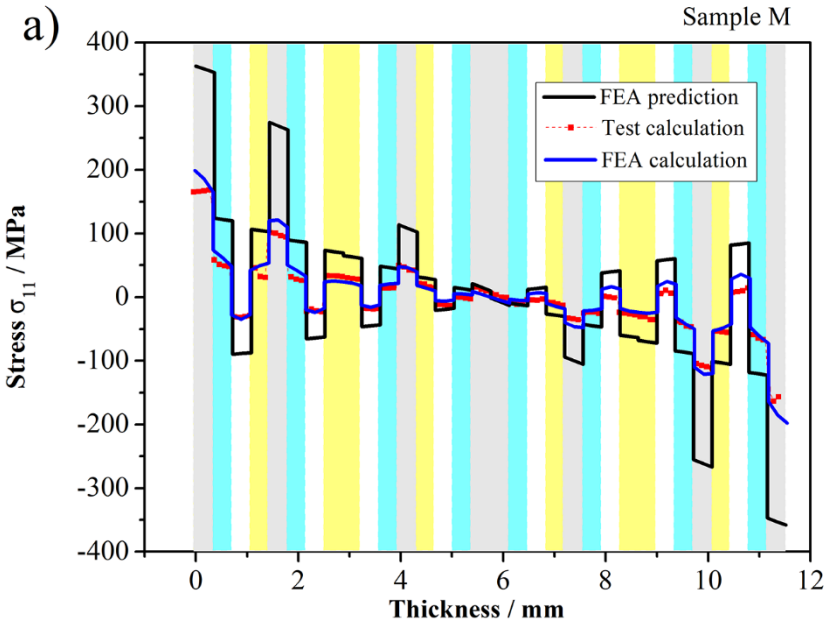

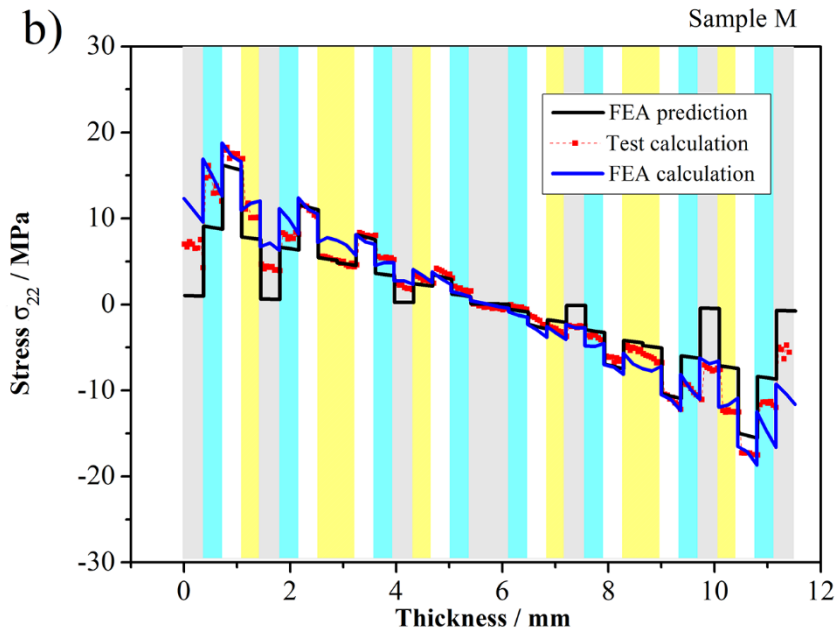

Fig. 13 Distribution of internal stresses at load level 4 for sample M: a) stress σ_{11}, b) stress σ_{22}

(notes: 0° layer, 90° layer, 45° layer, -45° layer)

However, the internal stresses and its distribution calculated based on the hole distortion obtained from both the physical DHD test measurements and the virtual DHD test simulations are strongly influenced by the stress calculation methods described in section 2.2. These results must be validated by the target value of assembly stresses predicted by the 3D laminated FEA model of the samples without the central hole under bending which resemble to the assembly stresses. The internal stresses predicted by FE without hole are also presented as FEA prediction in Fig. 12 and Fig. 13. FEA predictions are the internal stresses through thickness obtained directly from the FEA model simulating the assembly process with standard stress calculation method within the 3D FEA model, which represent the real assembly stresses. It is found that the agreement between calculation and the FE predicted bending stress is poor. The stresses calculated from measured and simulated distortions are generally much lower that the FEA predictions and the differences depend on the stress component layer orientation. For sample L in Fig. 12, the calculated σ_{11} stress component is about 70% of the FEA predictions in 0 degree layers. However, the calculated σ_{22} stress component is around 200% of

the FEA predictions in 90 degree layers. Significant differences are also found for the results of sample M in Fig. 13. The comparisons indicates that for the layup sequences used here, the stress calculation method used by Garza et al. [28,29] and presented in section 2.2 gives significant errors in the measurement of assembly stress. Consequently, an integrating calculation method is developed in the next section to improve the method given in section 2.2.

4. Development of the integrating calculation method and validations

4.1 Integrating calculation method

Composite laminates are generally manufactured with periodic stacking sequences to give layers with non-homogeneous properties within each layer. However, the classical stress analysis methods are generally based on the assumption that the non-homogeneous properties of the layers are smeared out in the global responses. Consequently, the deformation of the composite laminate can be analyzed in macro-scale with homogeneous mechanical properties as an orthotropic material which can be calculated as a one-layer block in the section 2.2, since the DHD test measurement technique can measure the variation of macro scale deformation, i.e. the changes of hole diameter through the thickness of the sample. Considering the characteristic feature of the global deformation and the local stress responses, a new calculation method is developed here by integrating the macro-scale deformation calculation based on Lekhnitskii's solution and layer-scale calculation of stresses with the anisotropic constitutive relation of composite laminate. The proposed calculation method flow chart is presented in Fig. 14. The Garza et al's [28,29] stress calculation method as given in section 2.2 is also included in Fig.14 for comparison.

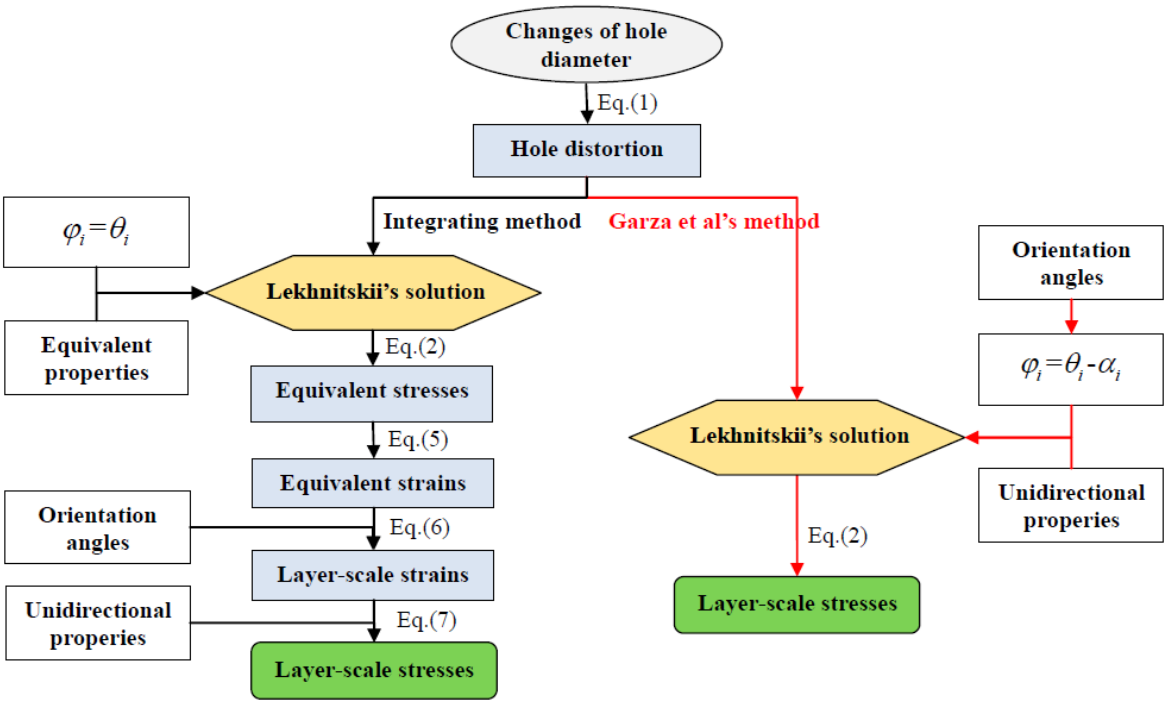

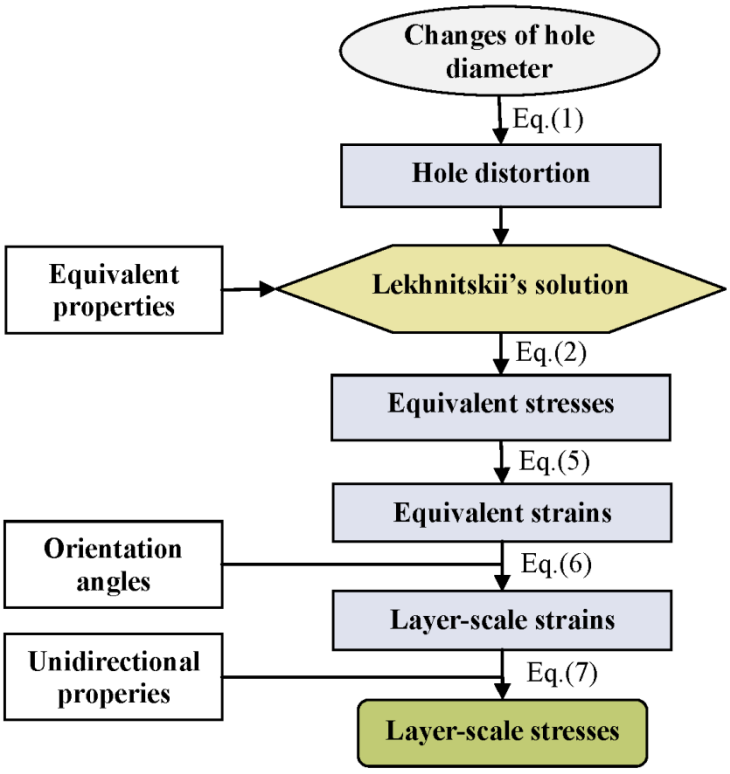

Fig. 14 Flow chart of the integrating calculation method

Firstly, hole distortions are calculated by Eq. (1). Then the equivalent internal stresses in global coordinate at each thickness, i.e. σ_{xx}, σ_{yy} and τ_{xy}, are calculated using Lekhnitskii's solution of Eq. (2) with the equivalent elastic constants of the laminate rather than the individual plies. Eq. (2) is solved using a standard least squares algorithm in Matlab. The equivalent elastic constants are calculated following Sun' s work [34] and listed in Tab. 3.

Afterwards, equivalent strains are derived with

$$\begin{bmatrix} \varepsilon_x \\ \varepsilon_y \\ \gamma_{xy} \end{bmatrix} = S \bullet \begin{bmatrix} \sigma_{xx} \\ \sigma_{yy} \\ \tau_{xy} \end{bmatrix} = \begin{bmatrix} S_{11} & S_{12} & 0 \\ S_{12} & S_{22} & 0 \\ 0 & 0 & S_{66} \end{bmatrix} \bullet \begin{bmatrix} \sigma_{xx} \\ \sigma_{yy} \\ \tau_{xy} \end{bmatrix} \tag{5}$$

where S is the equivalent compliance matrix of laminates, which can be calculated by

$$S = \begin{bmatrix} 1/E_x & -\nu_{xy}/E_x & 0 \\ -\nu_{xy}/E_x & 1/E_y & 0 \\ 0 & 0 & 1/G_{xy} \end{bmatrix}$$

where E_x, E_y, G_{xy} and ν_{xy} are the equivalent properties of the laminate.

Due to the compatibility of deformation between layers, layer scale strains are derived from the equivalent strains using the coordinate transfer matrix,

$$\begin{bmatrix} \varepsilon_{11} \\ \varepsilon_{22} \\ \gamma_{12} \end{bmatrix} = \left(T^{-1}\right)^T \bullet \begin{bmatrix} \varepsilon_x \\ \varepsilon_y \\ \gamma_{xy} \end{bmatrix} \tag{6}$$

where T denotes the coordinate transfer matrix:

$$T = \begin{bmatrix} \cos^2\alpha & \sin^2\alpha & 2\sin\alpha\cos\alpha \\ \sin^2\alpha & \cos^2\alpha & -2\sin\alpha\cos\alpha \\ -\sin\alpha\cos\alpha & \sin\alpha\cos\alpha & \cos^2\alpha - \sin^2\alpha \end{bmatrix}$$

where α is the orientation angle between the fibre direction and the global X direction.

Lastly, assuming conditions of plane stress, layer scale stresses are calculated by

$$\begin{bmatrix} \sigma_{11} \\ \sigma_{22} \\ \tau_{12} \end{bmatrix} = Q_0 \bullet \begin{bmatrix} \varepsilon_{11} \\ \varepsilon_{22} \\ \gamma_{12} \end{bmatrix} \tag{7}$$

where Q_0 is the layer scale stiffness matrix for the UD laminate, given by the inverse of the compliance matrix S_0. The compliance matrix can be obtained by

$$S_0 = \begin{bmatrix} 1/E_{11} & -\nu_{12}/E_{11} & 0 \\ -\nu_{12}/E_{11} & 1/E_{22} & 0 \\ 0 & 0 & 1/G_{12} \end{bmatrix}$$

where, E_{11}, E_{22}, G_{12} and ν_{12} are the elastic constants of the unidirectional laminates (see Tab. 2).

Following this procedure, the distribution of the layer scale stresses is reconstructed by carrying out the calculation at different positions through the thickness using the corresponding layer scale material properties.

Table. 3 Equivalent elastic constants of laminates

Property	**Value**		
	L:$[[0_2/90_2]_{4S}]_S$	**M**:$[[0_2/45_2/90_2/\text{-}45_2]_{2S}]_S$	**N**:$[45_2/\text{-}45_2]_{8S}$
E_x/GPa	75.81	53.49	14.26
E_y/GPa	75.81	53.49	14.26
E_z/GPa	9.34	9.34	9.34
G_{xy}/GPa	3.92	20.28	36.64
G_{xz}/GPa	3.24	3.24	3.24
G_{yz}/GPa	3.24	3.24	3.24
ν_{xy}	0.03	0.32	0.82
ν_{xz}	0.44	0.31	0.08
ν_{yz}	0.44	0.31	0.08

4.2 Validation of the integrating calculation method

It is demonstrated from above section in Fig.11 to Fig.13 that the changes of diameter and the calculated internal stress profiles obtained from the physical DHD measurements and virtual DHD simulations are very similar, apart from some local diversions from the physical DHD measurement.

Consequently, the numerical analysis methodology for the virtual DHD simulations presented in section 3.3 is used here to validate the ability of the integrating calculation method developed in above section to determine the internal stresses based on the changes of the diameter in DHD measurement. The results of an FE simulation of the DHD method using the modified calculation presented in section 4.1 are compared with the existing method of Garza et al. [28,29] described section 2.2 and the FE prediction of the bending stress. Results are provided for the two layups used previously, L and M, and an additional layup, layup N: $[45_2/\text{-}45_2]_{8S}$, to assess the performance of the modified method for a shear-resistance layup.

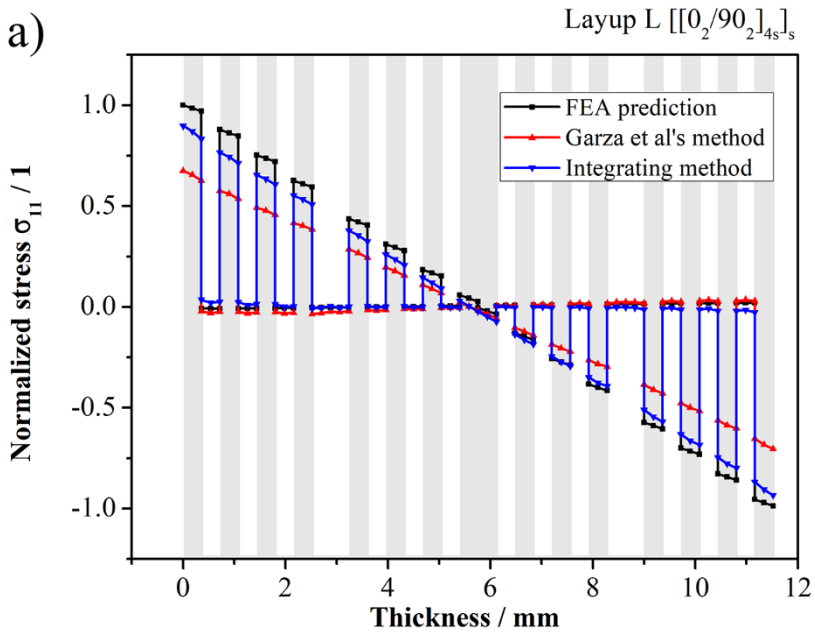

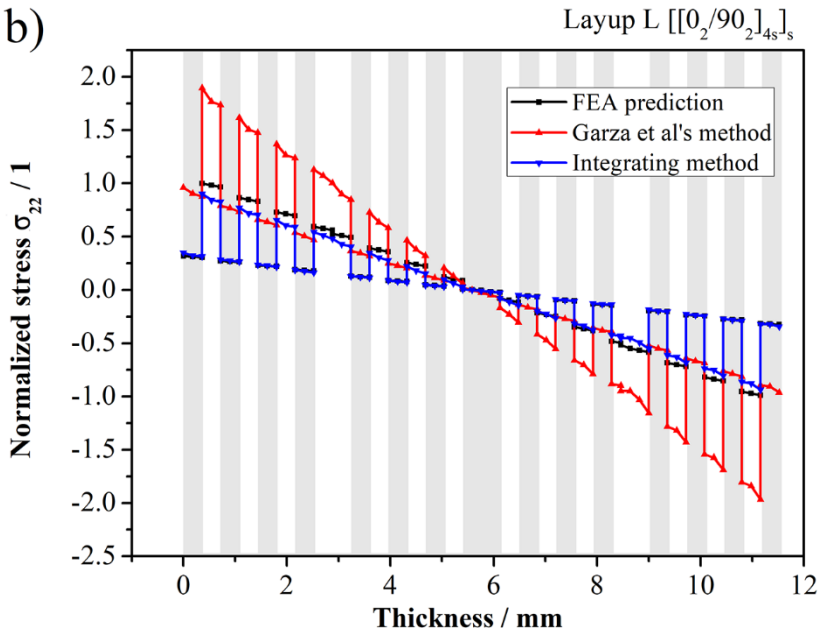

Fig. 15 Internal stresses calculated by different methods for layup L: a) stress σ_{11}, b) stress σ_{22}

(notes: 0° layer, 90° layer)

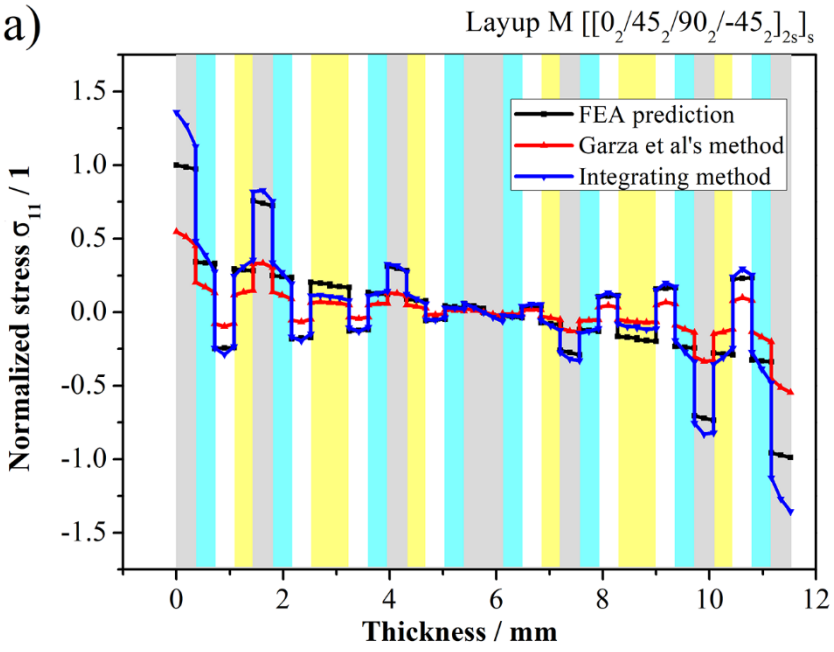

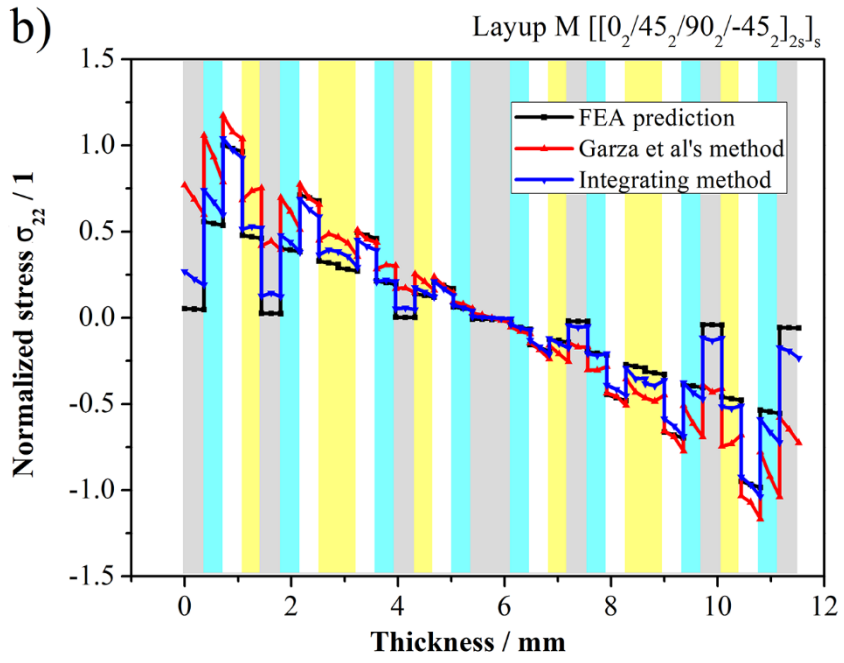

Fig. 16 Internal stresses calculated by different methods for layup M: a) stress σ_{11}, b) stress σ_{22}

(notes: 0° layer, 90° layer, 45° layer, -45° layer)

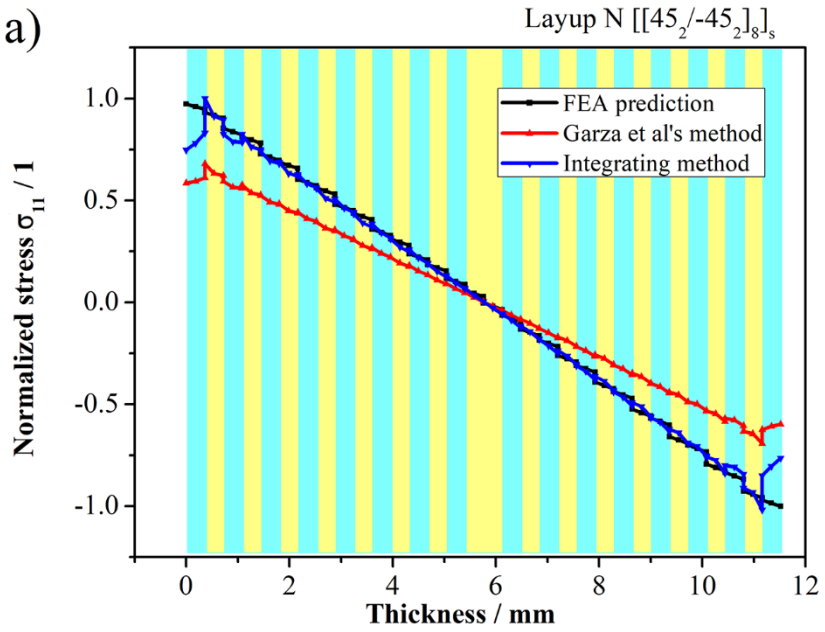

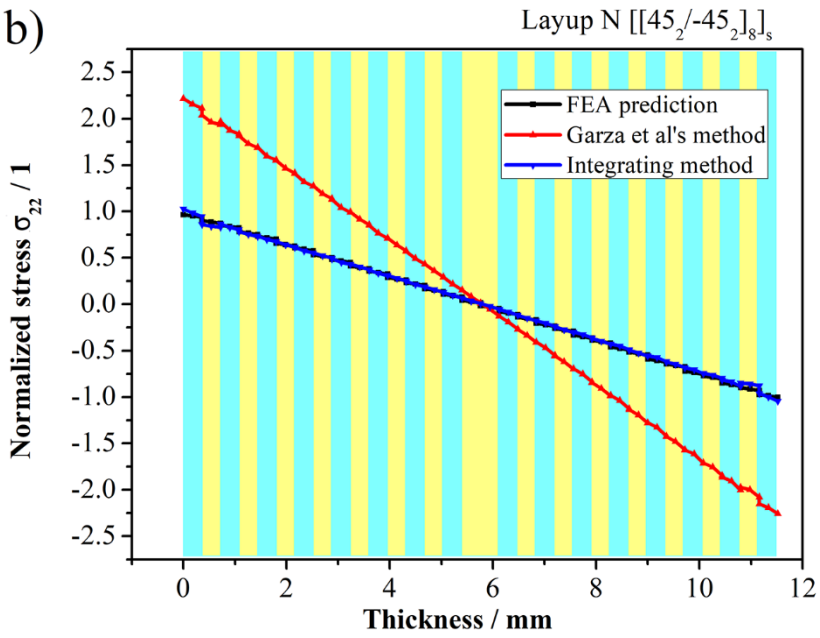

Fig. 17 Internal stresses calculated by different methods for layup N: a) stress σ_{11}, b) stress σ_{22}

(notes: 45° layer, -45° layer)

Internal stresses calculated by the different methods are presented in Fig. 15, Fig. 16 and Fig. 17 for layups L, M and N. The stresses are normalized by the maximum value of the bending stresses predicted by the 3D laminated FEM model. The internal stresses calculated by the proposed integrating method are in much better agreement with the FEA predictions than the stresses calculated by Garza et al.'s method. The global profiles of the internal stresses and their variation with ply orientation are both captured by the integrating calculation method developed in this study. Errors between FEA prediction and integrating calculations are less than 10%, except for near surface layers where the presence of the free surface results in larger hole distortions than are predicted by the DHD equations [33].

Based on the changes of hole diameter measured in physical test described in section 3, the through-thickness internal stress distributions are calculated using the new integrating calculation method. The results are compared with those of Garza et al. [28,29] and the bending stresses predicted by FEA in Fig. 18 for the sample with layup L at load level 4 and in Fig. 19 for sample M at load level 4.

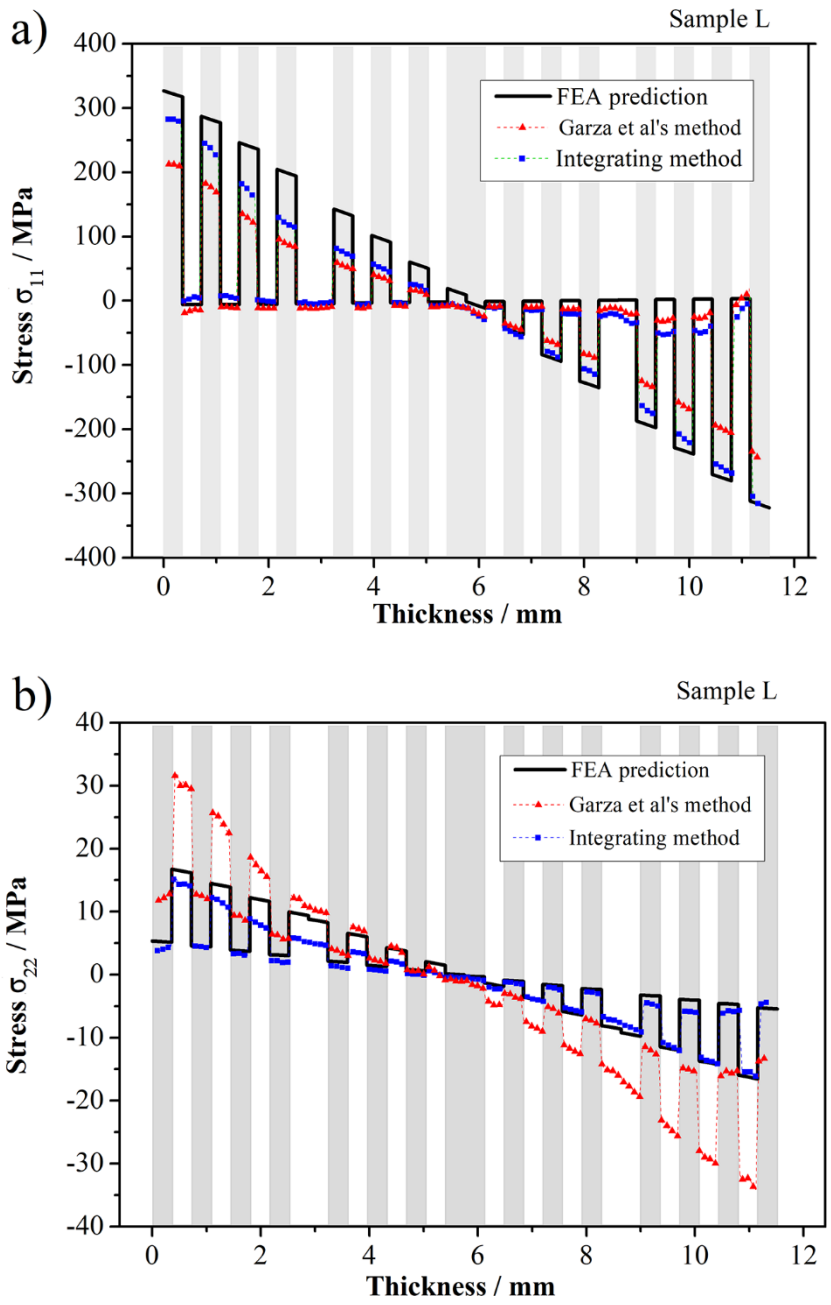

Fig. 18 Internal stresses calculated by integrating method at load level 4 for sample L: a) stress σ_{11}, b) stress σ_{22} (notes: 0° layer, 90° layer, 45° layer, -45° layer)

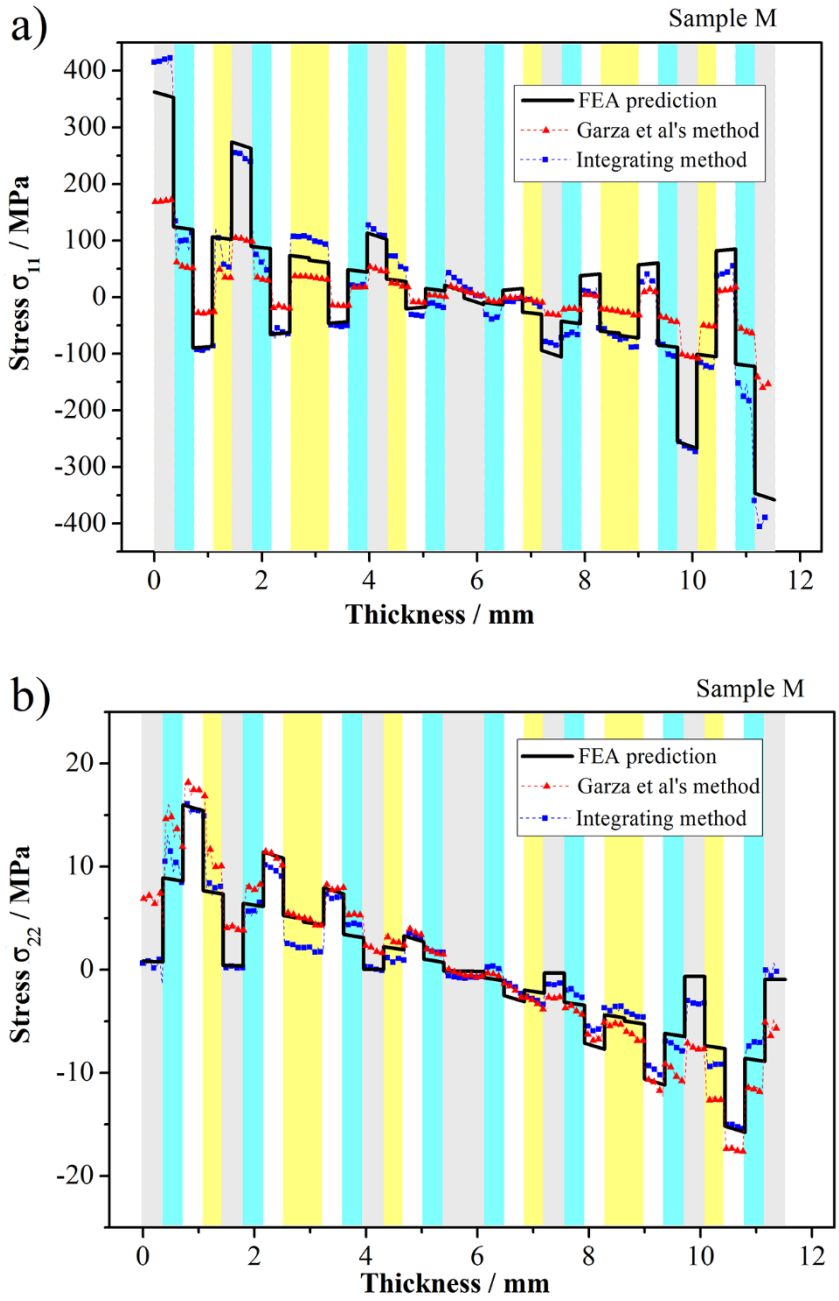

Fig. 19 Internal stresses calculated by integrating method at load level 4 for sample M: a) stress σ_{11}, b) stress σ_{22} (notes: 0° layer, 90° layer, 45° layer, -45° layer)

It can be observed that the integrating calculation method developed here provides a greatly improved DHD measurement of the stress, although some discrepancies can be seen for tensile stresses measured in sample L. This is due to that the changes of hole diameter measured in the test shows local deviation compared with the virtual DHD test simulations at 1/4 thickness as shown in Fig. 11 a).

The advantage of the proposed integrating calculation method is attributed to the combination of macro-scale and layer-scale analysis. The fundamental kinematics of the deformation in the beam theories commonly used in the engineering applications assumes deformation compatibility, i.e. continues displacement (strain) distribution through the beam thickness. For example, linear distribution of strain through the thickness is assumed in the classical beam theory (CBT) and the Timoshenko beam theory. For composite laminates under bending, continues strain distribution through thickness is still required even with discontinuous stress distribution due to the elastic property differences among different layers.

In the previous stress calculation method proposed by Garza et al, the layer-scale stresses in each individual block of the composite laminate is calculated directly from the hole distortion profile measured with the DHD technique and the orthotropic elastic properties of the ply orientation. There is not consideration of the global deformation compatibility, i.e. continues distribution of strain, through the thickness the composite laminate. In the new method proposed in this paper, the global deformation compatibility is considered by calculating the equivalent stress and then equivalent strain based on the hole distortion profile measured with the DHD technique and the global equivalent elastic properties of the composite laminate. Then the local strain is calculated based on the global equivalent strain, and the layer-scale discontinuous stresses are calculated with the orthotropic elastic properties of the ply orientation. The new two steps method which consider both the global deformation compatibility and the local layer-scale stress-strain relationship of composite laminate provide better solution compared with the previous method.

Generally, it is demonstrated that the integrating calculation method able to reconstruct the internal layer-scale stresses from central hole distortion obtained from the DHD measurement technique. Therefore, it is feasible to use the modified DHD technique to measure the manufacture assembly stresses of thick composite components for structural integrity assessment.

It is noted that in this work, measurements of the diameter of the reference hole which are made after trepanning in the standard DHD technique are replaced by measurements before application of loading. Therefore, in a practical application of the measurement of assembly stress with a trepan step, some hole distortion due to cure stress in the assembled composite components with occur. These hole distortions will superimpose on those due to assembly stress. According to previous studies [27,29], these cure stresses cannot be measured precisely using the DHD technique. The influence of these pre-existing cure stresses on the accuracy of the measurement of assembly stress requires further investigation. The modified DHD method, rather than the trepanning, was selected in this investigation due to its simplicity which can be easily used in engineering application. Trepanning method which normally requires accurate control of the trepanning process to achieve reliable measurement results is much more complex and time-consuming techniques. Other residual stress measurement methods such as incremental hole-drilling, slitting, or ring-core techniques combined with the inverse finite element analysis could also be potentially extended to measure the assembly stresses, even though those techniques are more complex compared with the current proposed method. With the feasibility of the proposed modified DHD method validated in this study, future work can be carried out to compare the advantage and disadvantage of this method and the other methods.

5. Conclusion

Inspired by the application of deep-hole drilling (DHD) method which is widely used to reconstruct residual stresses in thick metallic components, the feasibility to extend and modify the DHD method to measure the assembly stresses in composite components is explored in this research. The experimental and numerical simulation results from both the physical and virtual DHD test revealed that the proposed modified DHD techniques can capture the global profiles and their variation with ply orientations of the assembly stresses, however the previous stress calculation method used with the DHD technique leads to substantial errors in the magnitude of the internal stresses. Consequently, an

integrating stress calculation methodology is proposed, and the internal stresses calculated by the proposed integrating method with DHD technique are significantly improved and agree well with 3D FEM predictions. It is therefore demonstrated that the modified DHD techniques can be potentially used to quantify the through-thickness distribution of assembly stresses in thick composite laminates for safety and integrity assessment of composite structures.

Acknowledgements

The authors are grateful to Steve Harding and Matt Bland of the University of Bristol for providing technical support during the experiment work. This research was supported by the Foreign Science and Technology Cooperation Project of Hubei Provenience (Grant No. 2013BHE008), the China Postdoctoral Science Foundation (Grant No. 2018M632933) and the Fundamental Research Funds for the Central Universities (Grant No. 2018III066GX).

References

[1] Wisnom MR, Gigliotti M, Ersoy N, Campbell M, Potter KD. Mechanisms generating residual stresses and distortion during manufacture of polymer–matrix composite structures. Compos Part A Appl Sci Manuf 2006;37:522–9. https://doi.org/10.1016/J.COMPOSITESA.2005.05.019.

[2] Ding A, Li S, Wang J, Ni A. A new analytical solution for spring-in of curved composite parts. Compos Sci Technol 2017;142:30–40. https://doi.org/10.1016/J.COMPSCITECH.2017.01.024.

[3] Hu H, Cao D, Pavier M, Zhong Y, Zu L, Liu L, Li S. Investigation of non-uniform gelation effects on residual stresses of thick laminates based on tailed FBG sensor. Compos Struct 2018;202:1361–72. https://doi.org/10.1016/J.COMPSTRUCT.2018.06.074.

[4] Matveev MY, Belnoue JP-H, Nixon-Pearson OJ, Ivanov DS, Long AC, Hallett SR, Jones AI. A numerical study of variability in the manufacturing process of thick composite parts. Compos Struct 2019;208:23–32. https://doi.org/10.1016/J.COMPSTRUCT.2018.09.092.

[5] Antolin-Urbaneja JC, Livinalli J, Puerto M, Liceaga M, Rubio A, San-Roman A, Goenaga I. End-Effector for Automatic Shimming of Composites. SAE Technical Paper 2016:2016-01-2111. https://doi.org/10.4271/2016-01-2111.

[6] Jon Ostrower. Boeing says 787 shim repairs to take days, not months. Flight Glob 2012.

https://www.flightglobal.com/news/articles/boeing-says-787-shim-repairs-to-take-days-not-mont-367930/ (accessed February 8, 2012).

[7] D.D. Baker, D.P. Mooney. Boeing 787-8 Design, Certification, and Manufacturing Systems Reviews. Boeing, March 19, 2014.

[8] Sim R, Saadat M, Najafi F. Prediction of variation in wingbox assembly operation by finite element method. 2008 World Autom. Congr., Hawaii, USA: IEEE; 2008, p. 1–5.

[9] Locomachs project's webpage. Retrieved from: https://cordis.europa.eu/project/rcn/105426/factsheet/en.

[10] Yang Y, Wang Y-Q, Liu X, Gao H, Bao Y. The effect of shimming material on flexural behavior for composite joints with assembly gap. Compos Struct 2019;209:375–82. https://doi.org/10.1016/J.COMPSTRUCT.2018.10.086.

[11] D'Angelo G, Cavaccini G, Rampone S. Shimming Analysis of Carbon-Fiber Composite Materials with Eddy Current Testing. 2018 5th IEEE Int. Work. Metrol. Aerosp., Rome, Italy: IEEE; 2018, p. 68–73. https://doi.org/10.1109/MetroAeroSpace.2018.8453579.

[12] Söderberg R, Wärmefjord K, Lindkvist L. Variation simulation of stress during assembly of composite parts. CIRP Ann 2015;64:17–20. https://doi.org/10.1016/J.CIRP.2015.04.048.

[13] Wang H, Liu J. Tolerance simulation of composite wingbox assembly considering preloading-modified distribution. Assem Autom 2016;36:224–32. https://doi.org/10.1108/AA-08-2015-067.

[14] Wang H. Effect of Spring-in Deviation on Fatigue Life of Composite Elevator Assembly. Appl Compos Mater 2018;25:1357–67. https://doi.org/10.1007/s10443-017-9670-0.

[15] Yuksel O, Baran I, Ersoy N, Akkerman R. Investigation of transverse residual stresses in a thick pultruded composite using digital image correlation with hole drilling. Compos Struct 2019;223:110954. https://doi.org/10.1016/J.COMPSTRUCT.2019.110954.

[16] Wu X, Fuller JD, Longana ML, Wisnom MR. Reduced notch sensitivity in pseudo-ductile CFRP thin ply angle-ply laminates with central 0° plies. Compos Part A Appl Sci Manuf 2018;111:62–72. https://doi.org/10.1016/J.COMPOSITESA.2018.05.011.

[17] Di Sante R. Fibre Optic Sensors for Structural Health Monitoring of Aircraft Composite Structures: Recent Advances and Applications. Sensors 2015;15. https://doi.org/10.3390/s150818666.

[18] Das S, Saha P. A review of some advanced sensors used for health diagnosis of civil engineering structures. Measurement 2018;129:68–90. https://doi.org/10.1016/J.MEASUREMENT.2018.07.008.

[19] Salvetti M, Sbarufatti C, Gilioli A, Dziendzikowski M, Dragan K, Manes A, Giglio M. On the

mechanical response of CFRP composite with embedded optical fibre when subjected to low velocity impact and CAI tests. Compos Struct 2017;179:21–34. https://doi.org/10.1016/J.COMPSTRUCT.2017.07.063.

[20] Rito RL, Crocombe AD, Ogin SL. Health monitoring of composite patch repairs using CFBG sensors: Experimental study and numerical modelling. Compos Part A Appl Sci Manuf 2017;100:255–68. https://doi.org/10.1016/J.COMPOSITESA.2017.05.012.

[21] Zhandano IM, Gonchar AK. Determining the residual welding stresses at depth in metals. Autom Weld 1978;31:22–4.

[22] Beaney EM, Measurement of sub-surface stress, CEGB Report Rd/B/N4325; 1978.

[23] Smith DJ, Bouchard PJ, George D. Measurement and prediction of residual stresses in thick-section steel welds. J Strain Anal Eng Des 2000;35:287–305. https://doi.org/10.1243/0309324001514422.

[24] Kingston E, Stefanescu D, Mahmoudi A, Truman C, Smith D. Novel Applications of the Deep-Hole Drilling Technique for Measuring Through-Thickness Residual Stress Distributions. J ASTM Int 2006;3:1–12. https://doi.org/10.1520/JAI12568.

[25] Mahmoudi AH, Hossain S, Truman CE, Smith DJ, Pavier MJ. A New Procedure to Measure Near Yield Residual Stresses Using the Deep Hole Drilling Technique. Exp Mech 2009;49:595–604. https://doi.org/10.1007/s11340-008-9164-y.

[26] Smith DJ, Zheng G, Hurrell PR, Gill CM, Pellereau BME, Ayres K, Goudar D, Kingston E. Measured and predicted residual stresses in thick section electron beam welded steels. Int J Press Vessel Pip 2014;120–121:66–79. https://doi.org/10.1016/J.IJPVP.2014.05.001.

[27] Bateman MG, Miller OH, Palmer TJ, Breen CEP, Kingston EJ, Smith DJ, Pavier MJ. Measurement of residual stress in thick section composite laminates using the deep-hole method. Int J Mech Sci 2005;47:1718–39. https://doi.org/10.1016/J.IJMECSCI.2005.06.011.

[28] Garza C, Shterenlikht A, Pavier MJ, Smith DJ. Closed-form solutions of hole distortion for use in deep-hole drilling measurements of residual stress in orthotropic plates. J Strain Anal Eng Des 2016;52:77–82. https://doi.org/10.1177/0309324716675214.

[29] Garza C, Das R, Shterenlikht A, Pavier M. Measurement of assembly stress in composite structures using the deep-hole drilling technique. Compos Struct 2018;202:119–26. https://doi.org/10.1016/J.COMPSTRUCT.2017.12.031.

[30] Timoshenko S, Goodier JN. Theory of elasticity. McGraw Hill; 1951.

[31] Lekhnitskii SG. Anisotropic plates. Gordon and Breach; 1968.

[32] VEQTER Ltd, 8 Unicorn Business Park, Whitby Road, Brislington, Bristol BS4 4EX, United Kingdom. https://www.veqter.co.uk/

[33] Kingston, JE. Advances in the deep-hole drilling technique for residual stress measurement. University of Bristol, 2004. https://ethos.bl.uk/OrderDetails.do?uin=uk.bl.ethos.417630

[34] Sun CT, Li S. Three-Dimensional Effective Elastic Constants for Thick Laminates. J Compos Mater 1988;22:629–39. https://doi.org/10.1177/002199838802200703.

[35] Askri R, Bois C, Wargnier H. Effect of Hole-location Error on the Strength of Fastened Multi-Material Joints. Procedia CIRP 2016;43:292–6. https://doi.org/10.1016/J.PROCIR.2016.02.040.